Bioactive Materials 33 (2024) 562–571

Contents lists available at ScienceDirect

Bioactive Materials

journal homepage: www.keaipublishing.com/en/journals/bioactive-materials

An insect sclerotization-inspired antifouling armor on biomedical devices combats thrombosis and embedding

Nan Lyu [a,1], Daihua Deng [a,1], Yuting Xiang [a], Zeyu Du [a], Xiaohui Mou [a], Qing Ma [a], Nan Huang [a,b], Jing Lu [c,***], Xin Li [d], Zhilu Yang [a,d,e,**], Wentai Zhang [a,*]

[a] Dongguan Key Laboratory of Smart Biomaterials and Regenerative Medicine, Department of Cardiology, The Tenth Affiliated Hospital, Southern Medical University, Dongguan, Guangdong, 523059, China
[b] GuangZhou Nanchuang Mount Everest Company for Medical Science and Technology, Guangzhou, Guangdong, 510670, China
[c] Department of Anesthesiology, Sichuan Academy of Medical Sciences & Sichuan Provincial People's Hospital, School of Medicine, University of Electronic Science and Technology of China, Chengdu, Sichuan, 610072, China
[d] Department of Cardiology, Third People's Hospital of Chengdu Affiliated to Southwest Jiaotong University, Chengdu, Sichuan, 610072, China
[e] Guangdong Provincial Key Laboratory of Cardiac Function and Microcirculation, Southern Medical University, Guangzhou, Guangdong, 510080, China

ARTICLE INFO

Keywords:
Antifouling
Temporary interventional devices
Insect sclerotization
Phenol-polyamine chemistry
Universal armor

ABSTRACT

Thrombus formation and tissue embedding significantly impair the clinical efficacy and retrievability of temporary interventional medical devices. Herein, we report an insect sclerotization-inspired antifouling armor for tailoring temporary interventional devices with durable resistance to protein adsorption and the following protein-mediated complications. By mimicking the phenol-polyamine chemistry assisted by phenol oxidases during sclerotization, we develop a facile one-step method to crosslink bovine serum albumin (BSA) with oxidized hydrocaffeic acid (HCA), resulting in a stable and universal BSA@HCA armor. Furthermore, the surface of the BSA@HCA armor, enriched with carboxyl groups, supports the secondary grafting of polyethylene glycol (PEG), further enhancing both its antifouling performance and durability. The synergy of robustly immobilized BSA and covalently grafted PEG provide potent resistance to the adhesion of proteins, platelets, and vascular cells *in vitro*. In *ex vivo* blood circulation experiment, the armored surface reduces thrombus formation by 95 %. Moreover, the antifouling armor retained over 60 % of its fouling resistance after 28 days of immersion in PBS. Overall, our armor engineering strategy presents a promising solution for enhancing the antifouling properties and clinical performance of temporary interventional medical devices.

1. Introduction

Temporary interventional devices, such as inferior vena cava filters, embolic coils, balloon occlusion devices, and vascular plugs, have become essential tools in disease prevention and treatment [1–4]. However, these devices face the risk of thrombosis and retrieval difficulties due to tissue embedding, which can impair their efficacy and potentially result in fatal consequences [5–7]. It is believed that protein adsorption on devices is the main cause of these complications [8]. Upon introduced into the human body, these devices inevitably trigger a cascade of adverse events initiated by nonspecifically adsorbed proteins [9,10]. Accordingly, the development of strategies to prevent protein adhesion is crucial for the efficacy of temporary interventional devices. Antifouling surfaces have shown promise in mitigating protein attachment, thereby preventing surface fouling and its associated complications [11–13]. Various antifouling molecules have been explored for this purpose, including bovine serum albumin (BSA) [14,15], zwitterions [16,17], polyethylene glycol (PEG) [18], and fluoropolymers [19]. Among them, BSA emerges as a prominent candidate for surface modification applications. This natural protein, derived from bovine plasma,

Peer review under responsibility of KeAi Communications Co., Ltd.
* Corresponding author.
** Corresponding author. Dongguan Key Laboratory of Smart Biomaterials and Regenerative Medicine, Department of Cardiology, The Tenth Affiliated Hospital, Southern Medical University, Dongguan, Guangdong, 523059, China .
*** Corresponding author.
E-mail addresses: lujing.1979@hotmail.com (J. Lu), zhiluyang1029@smu.edu.cn (Z. Yang), zhang.wentai@foxmail.com (W. Zhang).
[1] These authors contributed equally to this work.

https://doi.org/10.1016/j.bioactmat.2023.12.004
Received 10 November 2023; Received in revised form 4 December 2023; Accepted 4 December 2023
2452-199X/© 2023 The Authors. Publishing services by Elsevier B.V. on behalf of KeAi Communications Co. Ltd. This is an open access article under the CC BY-NC-ND license (http://creativecommons.org/licenses/by-nc-nd/4.0/).

owns numerous advantages, such as wide availability, cost-effectiveness, and well-established purification method. Consequently, BSA-based coatings have found broad applications across fields including biomedical engineering [20], biosensing [21], drug delivery systems [22], and tissue engineering [23], offering indispensable solutions against biofouling challenges [24].

However, the broader application of BSA in antifouling coatings encounters challenges, particularly the lack of a facile method for stable surface fixation and its compromised antifouling activity in blood environments. Firstly, physical adsorption and covalent grafting are the two main methods to immobilize BSA onto biomaterial surfaces [25]. While physical adsorption is versatile for different surface shapes [26], its stability is often suboptimal [27]. In contrast, covalent grafting ensures strong anchoring of BSA to the surface, but it necessitates complex substrate pretreatment procedures [28]. Moreover, the antifouling effectiveness of BSA coatings may be compromised in physiological environments due to potential alterations in the charge properties of surfaces [29]. Therefore, creating a BSA coating that can be easily applied, stably adhered, and durably functioned is essential for enhancing the performance of temporary interventional medical devices.

The natural protective mechanisms observed in insects have recently inspired innovative approaches in biomedical surface modification [30]. Insects utilize a phenol oxidases-assisted phenol-polyamine chemistry to produce a robust exoskeleton. Notably, BSA can be viewed as a type of "polyamine" due to its formation via the polymerization of amino acids. Inspired by this, we develop an innovative solution to address the current limitations of BSA coatings. Our method integrates hydrocaffeic acid (HCA, phenol), BSA (polyamine), and sodium periodate (SP, oxidant) to construct a BSA-based armor on the surface of substrates. This armor is endowed with universal adhesive properties through the catechol groups present in HCA. Additionally, the abundant carboxyl groups in both BSA and HCA serve as secondary reaction sites, facilitating the grafting of amine-terminated PEG through a carbodiimide chemical reaction. PEG is well-known for its antifouling properties and, when grafted onto surfaces, creates a hydrating barrier on the BSA@HCA armor [31]. This additional layer further enhances the resistance to the adhesion of proteins, cells, and biomolecules, and also protects the underlying BSA armor from protease-induced degradation, ensuring the long-term efficacy of this antifouling armor in biological settings. The findings of this research not only pave the way for the use of biocompatible proteins in surface engineering but also hold promise in enhancing the efficacy of temporary interventional devices in clinical settings.

2. Materials and methods

2.1. Materials

BSA, HCA, glutaraldehyde, rhodamine, 4-Morpholineethanesulfonic acid (MES), N-hydroxy succinimide (NHS) and 1-(3-Dimethylaminopropyl)-3-ethylcarbodiimide hydrochloride (EDC) were obtained from Sigma-Aldrich. SP and toluidine blue were purchased from Shanghai Aladdin Bio-Chem Technology Co, LTD. Amine-terminated PEG (M_W = 5000 Da) were purchased from Macklin Inc, Shanghai, China. The cell culture media DMEM-F12, DMEM-High glucose, and fetal bovine serum (FBS) were purchased from GE Healthcare Life Sciences. The cell counting kit-8 (CCK-8) was purchased from DOJINDO. The ELISA kits were purchased from MULTI SCIENCES, Hangzhou, China and Beyotime Biotechnology, Shanghai, China. Mirror polished stainless steels (SS) was purchased from Corsair Medical Technology Co, Suzhou, China. The polyvinyl chloride (PVC) catheter for *ex vivo* thrombogenicity test was custom-made in Mingji Polymer Co, Jiangsu, China. Human umbilical artery smooth muscle cells (HUASMCs), Human umbilical vein endothelial cells (HUVECs) and the murine macrophage line RAW 264.7 (MCs) were purchased from the GuangZhou Jennio Biotech Co., Ltd.

2.2. Preparation of BSA@HCA armor

The BSA@HCA armor was prepared on various substrates, through a one-step dip-coating process. First, a mixed solution was prepared by mixing SP (2 mg mL^{-1}), BSA (3 mg mL^{-1}), and HCA (3 mg mL^{-1}) in distilled water. Then, the substrates were dipped into this mixture for 12 h at 37 °C. After reaction, the armored substrates were washed three times with distilled water and dried using nitrogen gas.

2.3. Covalent immobilization of PEG on BSA@HCA armor

The BSA@HCA armor was activated by using a water-soluble carbodiimide (WSC) system composed of EDC (5 mg mL^{-1}) and NHS (2.4 mg mL^{-1}) in a MES (9.76 mg mL^{-1}) buffer with pH ~ 5.4 for 30 min. Then, 5 mg mL^{-1} of PEG was added to the solution, and the reaction was allowed to proceed for 12 h. The coated substrates were then rinsed with PBS and distilled water, respectively, and labeled as PEG-BSA@HCA.

The mass quantification of PEG grafted to the armor was carried out using quartz crystal microbalance with dissipation (QCM-D, Q-sense AB, Sweden). First, the AT-cut 5 MHz quartz crystal with a 10 mm diameter of Au film was covered by BSA@HCA armor. The modified quartz crystal was then placed in the QCM-D chamber, and MES (pH ~ 5.4) solution was continuously injected at a rate of 30 μL min^{-1} until the baseline was stabilized. Afterwards, PEG was injected until the curve reached equilibrium. Subsequently, PBS (pH ~7.4) was perfused to remove any unbound PEG. The mass (Δm) of the grafted molecule was calculated using the Sauerbrey equation, whereby the frequency shift (Δf) of quartz crystal was converted into the mass change (Δm) of the electrode surface.

2.4. Characterization of the armor

The content of carboxy groups on the armors were measured by immersing in 5 × 10^{-4} M Toluidine Blue O at pH ~10 for 5 h. Then, unbound dye was removed with 1 × 10^{-4} M NaOH and the desorption of dye bound to carboxyl groups on armors was conducted with 50 % acetic acid solution. Absorbance at 633 nm was used for the colorimetry.

Attenuated total refraction fourier transform infrared spectroscopy (ATR-FTIR, Nicolet Model 5700) was utilized to analyze the chemical structure of the armor. Water contact angle (WCA) was measured at room temperature using a Krüss GmbH DSA 100 Mk 2 goniometer (Hamburg, Germany). Four parallel samples were selected for each group, and the average value was calculated. X-ray photoelectron spectroscopy (XPS) was used to analyze the chemical composition of the armor using K-Alpha from Thermo Electron (USA) with a monochromatic Al Kα (1486.6 eV) X-ray source, operating at a pressure of 12 kV and 15 mA, and a pressure of 3 × 10^{-7} Pa. The binding energy of C1s (284.5 eV) was designated as the reference for charge calibration.

2.5. Tribological test

The tribological test was performed employing a universal material tester (MFT-5000, Rtec-Instruments Inc., USA). The experiments were performed with rotation mode (rotation diameter: 8 mm; rotation speed: 360 rpm; normal load: 1 N) at 25 °C in liquid environment for 30 min.

2.6. Chemical stability of armor

The chemical robustness of the BSA@HCA armor was assessed by immersing it in different pH solutions at 37 °C. After incubation for 24 h, the absorbance value of the solution was measured at 480 nm, which was proportional to the amount of benzene ring in the solution and therefore allowed an indirect determination of the degradation of armor.

2.7. Cell culture

HUASMCs and HUVECs were cultured in DMEM-F12 medium supplemented with 10 % FBS. MCs were cultured in DMEM-High glucose medium supplemented with 5 % FBS.

2.8. Assays on the cell resistance of the antifouling armor

The resistance of antifouling armor against cell adhesion and growth behavior was evaluated by seeding cells onto test samples at a density of 2×10^4 cells mL^{-1} for 2, 24, and 72 h, respectively. The cells on the samples were then stained with Rhodamine 123 to visualize their morphology, and the proliferation viability of cells was measured using CCK-8 kit. The measurement of fibrinogen adhesion and activation, and cytokines release of MCs were performed using ELISA kits.

2.9. Cell migration

The ability of cells to migrate on the surface of the sample was assessed using the L-shaped gravity migration method [32]. Briefly, L-shaped 316L SS (0.8 cm × 2 cm) foil with one modified arm and one bare arm was prepared. Then, the bare arm was seeded at a density of 5×10^4 cells mL^{-1} for 6 h. After that, the sample was flipped over and placed in a fresh culture medium, causing the cells on the surface of the bare arm to migrate to the coated arm under the influence of gravity. Finally, the migrated cells were stained with Rhodamine 123 and visualized by the Leica DMRX fluorescence microscope after 24 h of incubation.

2.10. Ex vivo thrombogenicity test

The Local Ethical Committee and Laboratory Animal Administration Rules of China were strictly followed for all animal handling and surgical procedures. The animal experiments were approved by the Dongguan People's Hospital Laboratory Animal Welfare and Ethics Committee (Approval NO. IACUC-AWEC-202309003). Eight healthy New Zealand White rabbits (2.5–3.5 kg) were anesthetized by intravenous injection of 3 % pentobarbital sodium salt, and were used for *ex vivo* thrombogenicity test. To form a closed loop, the left carotid artery and the right jugular vein of the rabbit were connected by PVC catheter that contains bare and modified 316L SS foils (0.8 cm × 1.5 cm). After 2 h of blood circulation without anticoagulant, the samples were removed from the circulation system and rinsed with PBS. The occlusive rates of the catheter cross-sections were analyzed by photography, and the thrombus weight was calculated by weighing the tested sample. Additionally, the tested sample was fixed with glutaraldehyde (2.5 % in physiological saline) for SEM observation.

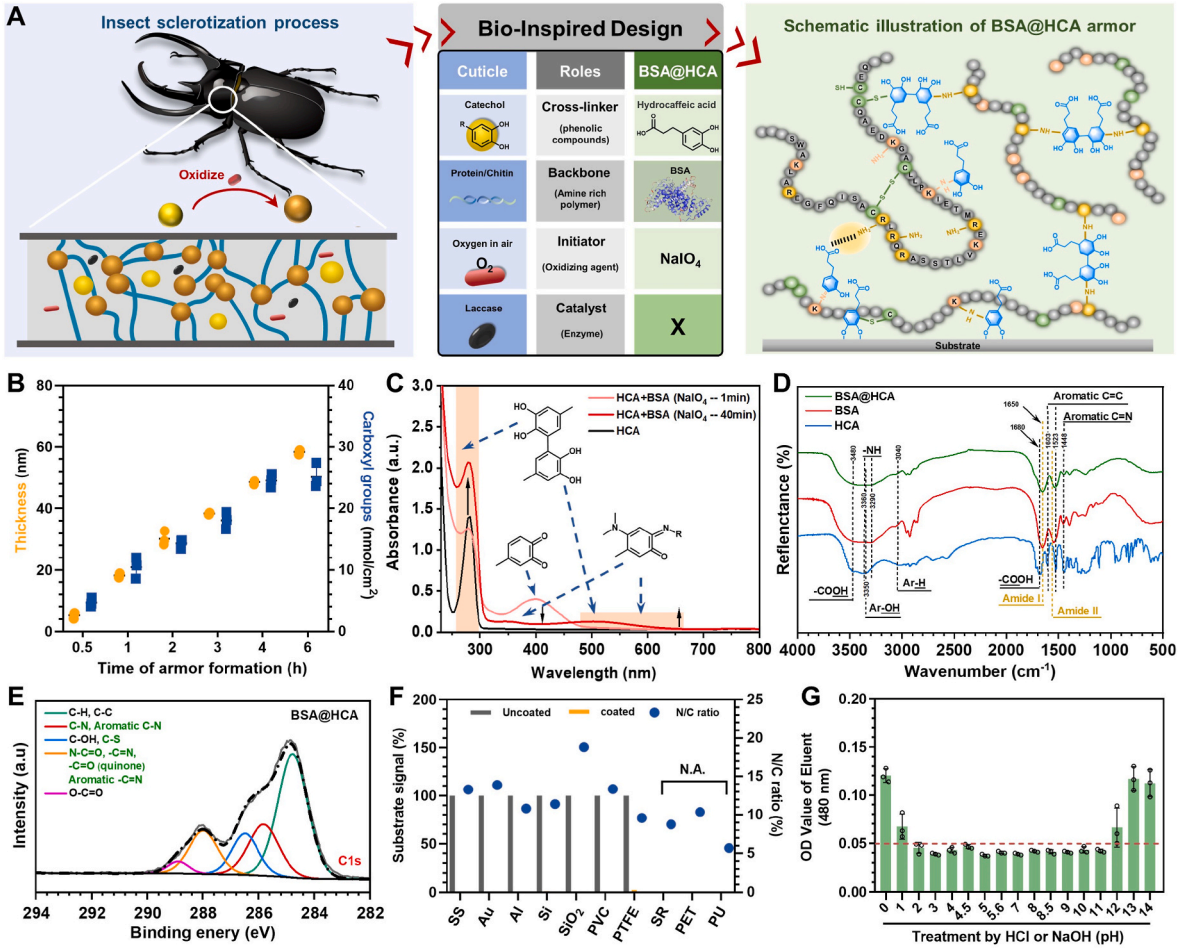

Fig. 1. Insect sclerotization-inspired phenol-polyamine chemistry for fabricating robust and universal BSA@HCA antifouling armor. (A) Sclerotization of insect cuticle (left) and formation mechanism of BSA@HCA armor (right). (B) Changes in the thickness and carboxyl group density of the BSA@HCA armor as a function of deposition time, ranging from 0.5 to 6 h. (C) UV–vis spectra of BSA and HCA mixed solution under SP-mediated oxidation. (D) GATR-FTIR spectra of HCA, BSA and BSA@HCA. (E) XPS high-resolution spectra of C1s for BSA@HCA armor. (F) XPS characterization of 10 different substrates before and after armoring with BSA@HCA. The characteristic XPS signals of the unmodified substrate was normalized to 100 %. Substrates with characteristic XPS signals indistinguishable from the BSA@HCA signal were marked by "N.A." (G) Degradation (OD 480 values > 0.05) of BSA@HCA armors in different pH environments.

3. Results and discussion

3.1. Preparation and characterization of antifouling BSA@HCA armor

To develop a facile method for the stable immobilization of BSA, our strategy draws inspiration from the sclerotization process observed in insects. We utilized HCA to crosslink with the inert protein BSA via phenol-polyamine chemistry under oxidizing environment (Fig. 1A). The phenolic hydroxyl groups in HCA could be oxidized to benzoquinone by SP, then readily reacting with both primary and secondary amine groups in BSA [33]. Meanwhile, BSA serves as a long-chain backbone, crosslinked by HCA, ensuring the stability of the armor. Owing to the adhesive nature of residual catechol groups in HCA, the resulting armor was expected to be firmly adhered to the substrates.

Firstly, the formation mechanism and characteristics of the BSA@HCA armor was investigated. After 30 min deposition, the thickness of the armor was only 5 nm (Fig. 1B). As the deposition time extended, there was a linear increase in thickness, reaching 60 nm after 6 h. A similar trend can be observed for the surface density of carboxyl groups. With the increasing of deposition time, the surface carboxyl groups gradually increased, peaking at 25 nmol cm^{-2} after 6 h. The abundant carboxyl groups on the surface provide sites for the following grafting of PEG. It is noteworthy that the surface carboxyl groups showed negligible variation after 4 h deposition, suggesting the full coverage of the armor on the substrate. To deeper understand the formation mechanism of the BSA@HCA armor, we examined the chemical structure changes in HCA during armor formation using UV–vis spectroscopy. It can be observed that the absorbance value at ~390 nm significantly increased after 1 min (Fig. 1C), indicating the conversion of o-phenol to the *o*-benzoquinone group in an oxidizing condition [33,34]. High performance liquid chromatography-mass spectrometry (HPLC-MS) provided further evidence that under oxidizing conditions, HCA converted to *o*-benzoquinone and dicatechol structures (Fig. S1). With the reaction proceed, the absorption peak attributed to the *o*-benzoquinone group diminished. Instead, peaks associated with structures featuring aromatic C–N and aromatic C═N emerged. This shift can be mainly attributed to the phenol-polyamine reactions between HCA and BSA [33]. The chemical composition and structure of BSA@HCA armor were detected by FTIR and XPS. As shown in Fig. 1D, the presence of characteristic peaks of BSA (Amine I and Amine II at 1660 and 1522 cm^{-1}, respectively) and HCA (aromatic C═C at 1603 and 1523 cm^{-1}) indicated the successful fabrication of the armor. Moreover, the peaks of aromatic C═N at 1448 cm^{-1} observed in BSA@HCA verified the phenol-polyamine crosslinking between BSA and HCA. XPS analysis further confirmed this crosslinking as evidenced by the presence of aromatic C═N, aromatic C–N, and N–C═O peaks (Fig. 1E and Fig. S2).

To verify the universal adhesive properties of the BSA@HCA armor, we applied it on various substrates commonly used in medical devices. It can be observed that all the substrates exhibited a color change after armoring, indicating the successful fabrication of the armor (Fig. S3). The surface elemental composition of modified samples was also detected using XPS (Fig. 1F and Fig. S4). As illustrated, the armor completely covered the signals from metallic and inorganic materials, confirming its full and uniform coverage. However, the characteristic elemental signals of carbon-based polymeric materials such as silicone rubber (SR), poly (Ethylene Terephthalare) (PET), and polyurethane (PU) were similar to that of the armor and thus difficult to be distinguished. Nevertheless, a consistent N/C ratio was observed after armoring for all the substrates, suggesting the universal adhesive properties of the BSA@HCA armor.

Importantly, the BSA@HCA armor exhibited impressive chemical stability under both acidic and alkaline environments. As shown in Fig. 1G, the armor remained intact across a pH range from 2 to 11. However, when the pH was below 1 or above 11, there was a significant increase in the optical density (OD) value of the eluent. This rise is mainly attributed to the disruption of the armor and the subsequent liberation of benzene ring in HCA to the eluents [35]. Furthermore, the long-term stability of the BSA@HCA armor is crucial for its antifouling performance. Therefore, we investigated both the morphology and thickness changes of the BSA@HCA armor after 28 days immersion in PBS. Scanning electron microscopy (SEM) analysis revealed that the BSA@HCA armor maintained its surface integrity without morphological alterations after 28 days immersion (Fig. S5). Moreover, the thickness of the armor exhibited negligible decrease during immersion. These results highlight the robustness of the BSA@HCA armor and its suitability for enhancing the surface properties of temporary biomedical devices.

3.2. Surface grafting of PEG on BSA@HCA armor

In pursuit of further enhancing the antifouling efficacy and durability of the BSA@HCA armor, a secondary grafting of PEG was performed, facilitated by carbodiimide reaction between carboxyl group (provided by BSA and HCA) and amine group (PEG) (Fig. 2A). It has been reported that the grafting amount is critical for the antifouling efficacy of PEG coating [36–39]. Thus, we first assessed the grafting quantity of PEG on the BSA@HCA armor using QCM-D. It can be observed that the highest grafting density of 510 ng cm^{-2} was achieved after 5 h of reaction (Fig. 2B). Such densely grafted PEG significantly increased the surface hydrophilicity (Fig. 2C). Specifically, the WCA for SS and BSA@HCA armor was 66.8 ± 5.2° and 76 ± 3.4°, respectively. Remarkably, after grafting with PEG, the WCA decreased to approximately 44.6 ± 3.4°. Considering the passive antifouling surface is realized by the formation of surface hydration layer, the enhanced hydrophilicity is believed to benefit its antifouling effectiveness [38,39].

To ascertain the covalent grafting of PEG, we conducted RA-FTIR and XPS analyses. As shown in Fig. 2D, the enhancement of characteristic peaks of –OH (at 3420 cm^{-1}) and C–*O*–C (at 1278, 1240, 1150, and 1100 cm^{-1}) was observed for PEG-BSA@HCA. Such enhancement can be ascribed to the presence of the PEG, indicating its successful grafting. Additionally, the characteristic peak of C–OH in the carboxyl group at 1393 cm^{-1} significantly decreased, suggesting the covalent grafting of PEG to the carboxyl groups through carbodiimide reaction. The chemical composition of PEG-BSA@HCA was further analyzed using XPS high-resolution spectra of C1s, N1s, and O1s. As depicted in Fig. 2E, after grafting with PEG, there was a notable decrease in peak intensity associated with C–N, C–O, and C═O bonds present in the BSA@HCA armor. Also, a remarkably decreased N1s peak in PEG-BSA@HCA was observed as compared to BSA@HCA (Fig. 2F and Fig. S6). These declines can be mainly caused by the limited detection depth of XPS and the complete coverage of PEG. This conclusion can be further supported by the significant increase in peak intensity of C–*O*–C bond after grafting with PEG in C1s and O1s (Fig. 2G). Overall, these findings confirm the successful grafting of PEG on the BSA@HCA armor via carbodiimide reaction [40,41].

It has been well recognized that the biomedical devices with high surface friction can harm endothelial cells during intervention, thereby elevating the risk of injuries and thrombosis [42–44]. Therefore, we measured the friction coefficients of SS, BSA@HCA, and PEG-BSA@HCA under wet conditions. As illustrated in Fig. 2H, PEG grafted samples exhibited substantially reduced friction coefficient under wet condition, implying a decreased potential for blood vessel damage. Such effects can be mainly attributed to the hydration layer formed on PEG-BSA@HCA and the brush-like structure of PEG [45].

3.3. Antifouling properties of PEG-BSA@HCA against HUVECs, HUASMCs and MCs

Cell adhesion on temporary intervention devices can be detrimental. Firstly, the accumulation of inflammatory cells to the implanted devices can trigger inflammations, which may lead to intervention failure [46].

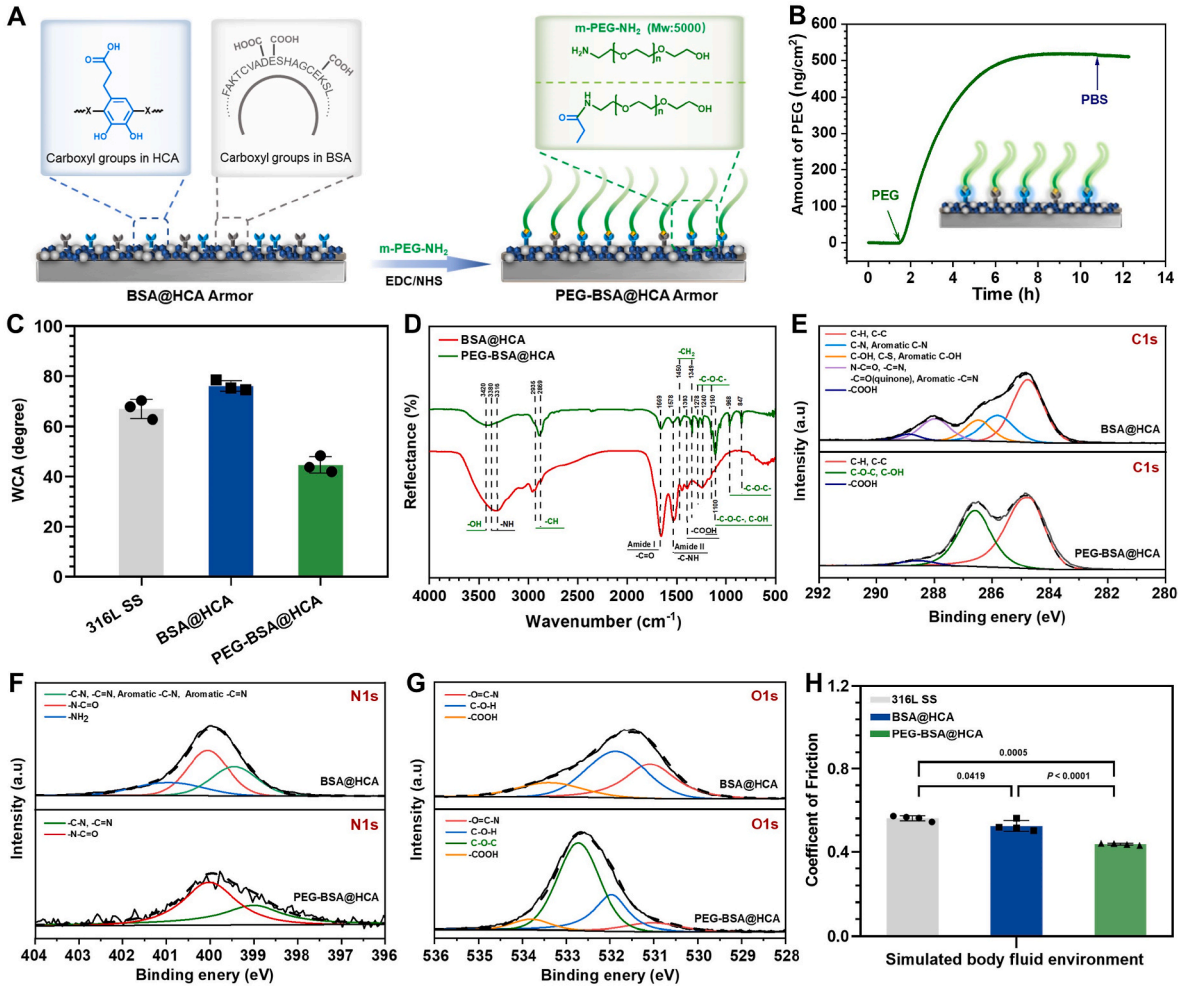

Fig. 2. Surface grafting of PEG on BSA@HCA armor. (A) Surface grafting of PEG through carbodiimide chemistry. (B) Real-time monitoring of the grafting amount of PEG determined by QCM-D. (C) WCA of 316L SS before and after armoring and grafting. (D) GATR-FTIR spectra of BSA@HCA and PEG-BSA@HCA. XPS high-resolution spectra of (E) C1s, (F) N1s, and (G) O1s for BSA@HCA and PEG-BSA@HCA. (H) Friction coefficient of 316L SS before and after armoring and grafting under wet conditions.

Additionally, the attachment and proliferation of vascular cells on devices such as inferior vena cava filters and vascular occluders might accelerate devices embedding, thus narrowing the safe retrieval window. Accordingly, the adhesion behavior and subsequent responses of vascular and inflammatory cells on the PEG-BSA@HCA armor was assessed *in vitro*.

HUVECs were first seeded on the samples and the adherent cells were characterized. As shown in Fig. 3A, the BSA@HCA armor exhibits a significant reduction in HUVECs adhesion compared to 316L SS, demonstrating the antifouling capacity of our BSA-based armor. Note that this resistance to the HUVECs adhesion was further enhanced after PEG grafting. Quantitative results showed that the PEG-BSA@HCA exhibited a tenfold reduction in HUVECs adhesion compared to SS, confirming its potent anti-adhesion capacity (Fig. 3B). This can be ascribed to the hydrated layer formed on the surface, serving as a barrier against cell attachment. Moreover, the PEG-BSA@HCA effectively inhibited cell proliferation (Fig. 3C and D) and migration (Fig. 3E and Fig. S7). Specifically, the migration distance on BSA@HCA and PEG-BSA@HCA armors decreased to 589.8 μm and 304.7 μm, respectively, compared to the distance of 692.5 μm on the 316L SS. Such effects might be associated with the reduced proteins on the surface that could promote cell proliferation and migration [47].

The adhesion and proliferation of HUASMCs on the samples was subsequently assessed. The response of HUASMCs on different samples was similar to that of HUVECs. Both the BSA@HCA and PEG-BSA@HCA armors significantly resisted the adhesion of HUASMCs, with the PEG-BSA@HCA surface proving more effective (Fig. 4A and B). Meanwhile, the proliferation of HUASMCs was also remarkably inhibited by both BSA@HCA and PEG-BSA@HCA (Fig. 4C and D). After 72 h incubation, the number of HUASMCs on the SS surface was 2.7-fold higher than on BSA@HCA, and 6.8-fold higher than on PEG-BSA@HCA. Similarly, the BSA@HCA and PEG-BSA@HCA surfaces notably suppressed cell migration from 609.6 μm to 447.1 μm and 257.7 μm, respectively (Fig. 4E and Fig. S7).

The introduction of vascular interventional devices can trigger a cascade of immune responses, which often include the recruitment of immune cells and activation of signaling pathways [48–50]. MCs, as one of the first responders in inflammation, are commonly used to evaluate the inflammatory response of biomedical devices [51]. Accordingly, we assessed the attachment and cytokine release of RAW 264.7 MCs on different samples. It can be observed that the BSA@HCA armor did not show a significant reduction in the adhesion of MCs compared to 316L SS after 24 h incubation (Fig. 5A and B). However, a notable inhibition of MCs proliferation on the BSA@HCA armor was evident after 72 h. Notably, the PEG-BSA@HCA exhibited a significant decrease in both adhesion and proliferation of MCs. Specifically, the fluorescence area of MCs on the PEG-BSA@HCA surface was just one-tenth of that on SS, demonstrating its potent antifouling properties. In the cytokine release

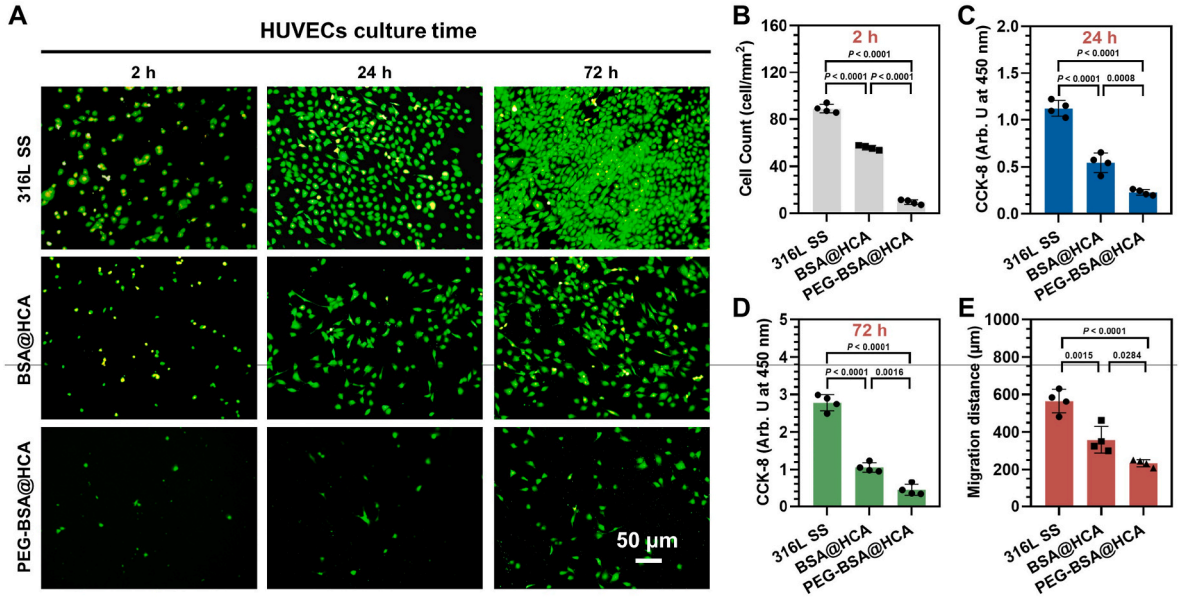

Fig. 3. Antifouling properties of PEG-BSA@HCA against ECs. (A) Fluorescence staining of HUVECs on different samples after 2, 24 and 72 h of culture. (B) Cell counting of HUVECs after 2 h of culture. (C, D) The proliferation of HUVECs after 24 and72 h of culture. (E) Migration distance of HUVECs on different samples after 1 day of incubation.

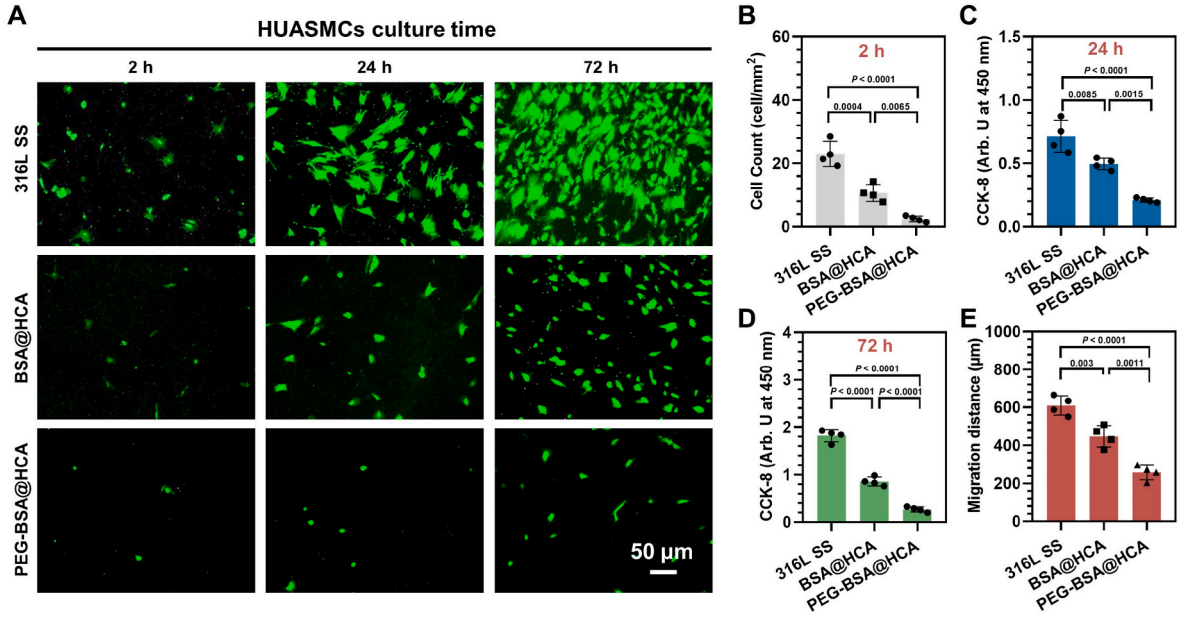

Fig. 4. Antifouling properties of PEG-BSA@HCA against SMCs. (A) Fluorescence staining of HUASMCs on different samples after 2, 24 and 72 h of culture. (B) Cell counting of HUASMCs after 2 h of culture. (C, D) The proliferation of HUASMCs after 24 and 72 h of culture. (E) Migration distance of HUASMCs on different samples after 1 day of incubation.

assay, neither BSA@HCA nor PEG-BSA@HCA triggered an elevation in cytokine levels, including TNF-α, IL-6, IL-10, and TGF-β, suggesting a favorable inflammatory response (Fig. 5C–F).

3.4. *In vitro and ex vivo antithrombogenic properties*

The risk of coagulation is a significant concern for implanted medical devices, as excessive clotting can lead to serious complications such as thrombosis, embolisms, and blockages within the device. The adhesion and activation of fibrinogen (Fg) and platelets are key factors in the coagulation process [52]. Therefore, we assessed the effectiveness of the PEG-BSA@HCA armor in inhibiting the adhesion and activation of fibrinogen and platelet.

Firstly, the samples were exposed to the platelet-poor plasma for evaluating the adhesion and activation of Fg. As illustrated in Fig. 6A, the BSA@HCA armor slightly reduced Fg adhesion and activation compared to 316L SS. Specifically, fibrinogen adhesion on BSA@HCA was 80.2 % relative to 316L SS, while its activation was lowered to 71.3 % of the 316L SS. Notably, PEG grafting considerably enhanced this effect. The introduction of PEG molecular brushes led to a remarkable decrease in fibrinogen adhesion on PEG-BSA@HCA, to just 58.8 % compared to 316L SS, and fibrinogen activation was significantly reduced to 35.8 % of 316L SS, indicating its superior anti-adhesion and anti-activation properties against Fg. In addition, we exposed the

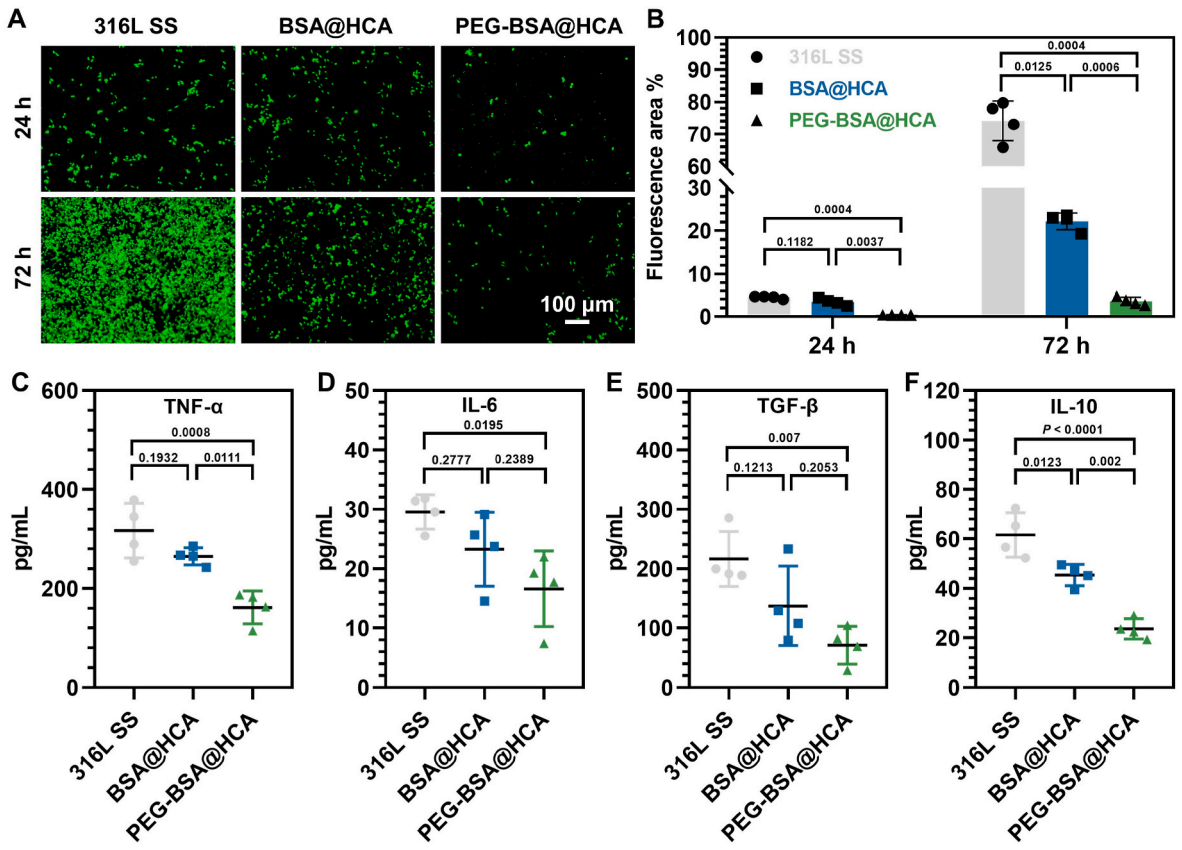

Fig. 5. Antifouling properties of PEG-BSA@HCA against inflammatory cells. (A) Fluorescence staining of RAW 264.7 MCs on different samples after 24 and 72 h of culture. (B) Quantification of fluorescence area of RAW 264.7 MCs on different samples after 24 and 72 h of culture. Cytokine release, including (C) THF-α, (D) IL-6, (E) TGF-β, and (F) IL-10, of RAW 264.7 MCs on different samples after 6 h of incubation.

samples to platelet-rich plasma to investigate the platelet responses in the presence of Fg. SEM images revealed a notable quantity of activated platelets, identified by their extended pseudopodia, on the surface of 316L SS as shown in Fig. 6B. Conversely, the BSA@HCA exhibited a remarkable reduction in platelet adhesion. Moreover, the few adhered platelets were predominantly in an inactivated state. This inhibitory effect was more pronounced in the case of the PEG-BSA@HCA, which displayed a substantial decline in platelet adhesion and activation. The quantification of the adhered and activated platelets was consistent with the SEM observation, further confirming the superior antifouling properties of the PEG-BSA@HCA (Fig. 6C).

To evaluate the anti-thrombotic properties of PEG-BSA@HCA armor, an *ex vivo* catheter blood circuits experiment was performed (Fig. 6D). As described in our previous work [52], the bare and modified 316L SS foils were placed in the PVC catheters, which are connected to a rabbit arteriovenous shunt. After 2 h of circulation, the samples were taken out and their anti-thrombotic properties were evaluated. As shown in Fig. 6E, severe thrombus formation was observed for SS, while only slight clotting was observed for the BSA@HCA. Notably, almost no clotting was formed on PEG-BSA@HCA, indicating its excellent anti-thrombotic properties. Quantitative analysis further confirmed this observation, as evidenced by the significant reduction of PEG-BSA@HCA in occlusion rate (Figs. 6F and 5.9 % vs. 100 %), thrombus weight (Figs. 6G and 3.3 mg vs. 35.8 mg), and blood flow rate (Figs. 6H and 92.6 % vs. 37.6 %) compared to SS. SEM observation provided further evidence, revealing the aggregation of erythrocytes and platelets and fibrous-like thrombus on the SS surface. In contrast, the PEG-BSA@HCA surface showed only a small presence of red blood cells, confirming the thrombogenesis inhibition of the antifouling armor (Fig. 6I).

3.5. Durability of PEG-BSA@HCA antifouling armor

The durability of antifouling properties is critical to the long-term efficacy of implanted devices. In this study, we tested the durability of the PEG-BSA@HCA antifouling armor by pre-immersion in PBS for 1, 4, 7, 14, and 28 days respectively. After treatment by PBS, the *ex vivo* catheter blood circuits and *in vitro* cell adhesion and proliferation experiments were performed. It can be observed that the PEG-BSA@HCA armor demonstrated a slight reduction in antithrombotic efficiency in *ex vivo* catheter blood circuits after prolonged immersion (Fig. 7A). However, it maintained substantial effectiveness assessed by occlusion ratio, thrombus weight, and blood flow rate, with more than 70 % of its initial capacity preserved after 28 days immersion (Fig. 7B). These results indicate its superior stability in antithrombosis. Similar trend can also be observed for the adhesion and proliferation of vascular and inflammatory cells. As illustrated in Fig. 7C–H, with the increase of immersion time, the anti-adhesion and anti-proliferation capacity of the PEG-BSA@HCA slightly decreased. Whereas, after immersion in PBS for 28 days, the anti-adhesion and anti-proliferation capacity against HUVECs, HUASMCs, and MCs is still above 60 %, indicating its durable antifouling properties.

It is noteworthy that the retention of antifouling efficacy varied among cell types. For ECs and MCs, the capacity to prevent adhesion and proliferation dropped to between 60 % and 70 % after 28 days. In contrast, for SMCs, the retention was still higher than 70 %. The varying antifouling durability against different cell types can mainly be attributed to their different sizes in this work. The typical sizes of ECs, SMCs, and MCs are approximately 10–50 μm, 20–200 μm, and 10–20 μm, respectively. As the immersion time increases, the grafting density of PEG would gradually decrease due to the degradation of the BSA@HCA armor. This leads to larger gaps between PEG chains, making it easier for

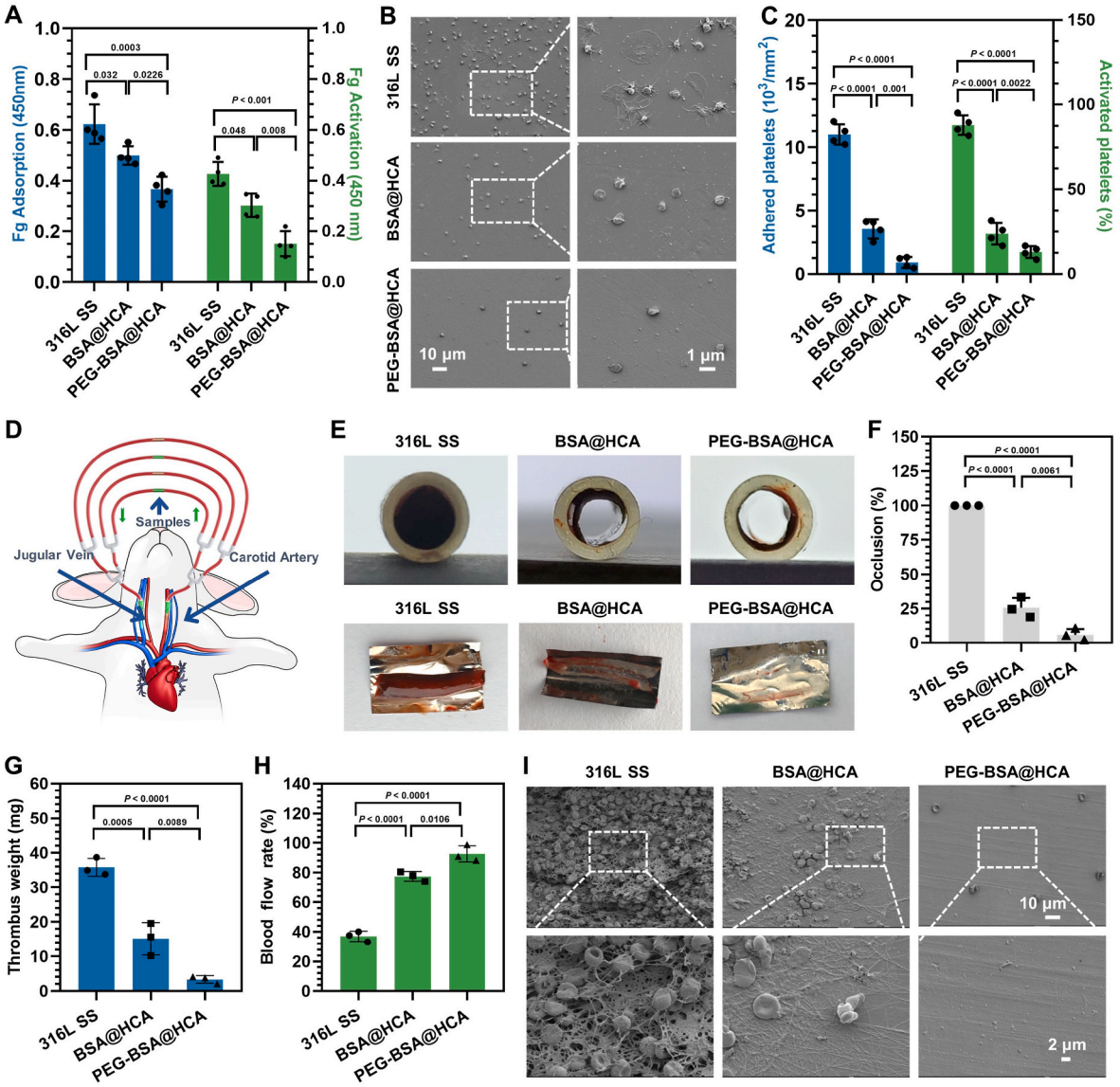

Fig. 6. *In vitro* and *ex vivo* antithrombogenic properties of PEG-BSA@HCA. (A) Relative quantification of Fg adsorption and activation (determined by γ chain exposure) on 316L SS, BSA@HCA and PEG-BSA@HCA. (B) Morphology of adhered platelets on the samples surfaces observed by SEM. (C) Relative quantification of adherent and activated platelets on samples surfaces. (D) Schematic illustration of rabbit carotid arteriovenous shunt model. (E) Cross-sectional and surface images of bare and modified 316L SS foils after circulation. Quantitative results of (F) occlusion, (G) thrombus weight, and (H) blood flow rate of different samples. (I) SEM images of samples surfaces after circulation.

smaller cells, such as ECs and MCs, to adhere to the substrate. In contrast, the antifouling properties of PEG-BSA@HCA demonstrated higher retention against the SMCs with larger size. In comparison, the antifouling performance of the BSA@HCA armor declined markedly post-immersion (Figs. S9–S11). Meanwhile, no significant varying antifouling durability was observed among different cells. Despite this, the antifouling properties of BSA@HCA remained superior to that of SS.

4. Conclusions

In this study, we present a facile approach for developing universal and durable antifouling armor for temporary interventional biomedical devices. By mimicking the insect sclerotization process, we develop a one-step process to crosslink BSA with HCA under oxidizing condition via phenol-polyamine chemistry. The resultant armor exhibits universal adhesive capabilities on various substrates (e.g., metals, inorganics, and polymers). Moreover, BSA, serving as the structural backbone, endows the armor with superior stability, which maintains its integrity in PBS after 28 days immersion. To further enhance the durability and antifouling performance, we graft PEG onto the carboxyl-rich BSA@HCA armor. This grafting significantly elevates the antifouling efficacy of PEG-BSA@HCA, potently resisting the adhesion of proteins and platelets, as well as inhibiting the attachment and proliferation of ECs, SMCs, and MCs *in vitro*. In *ex vivo* blood circulation assays, the armored surface exhibited a 95 % reduction in thrombus formation. Remarkably, even after 28 days in PBS, the antifouling armor retained over 60 % of its initial fouling resistance. Overall, our armor engineering strategy presents a promising solution for enhancing the antifouling properties and clinical performance of temporary interventional medical devices.

Data availability Statement

The data that support the findings of this study are available from the corresponding authors upon reasonable request.

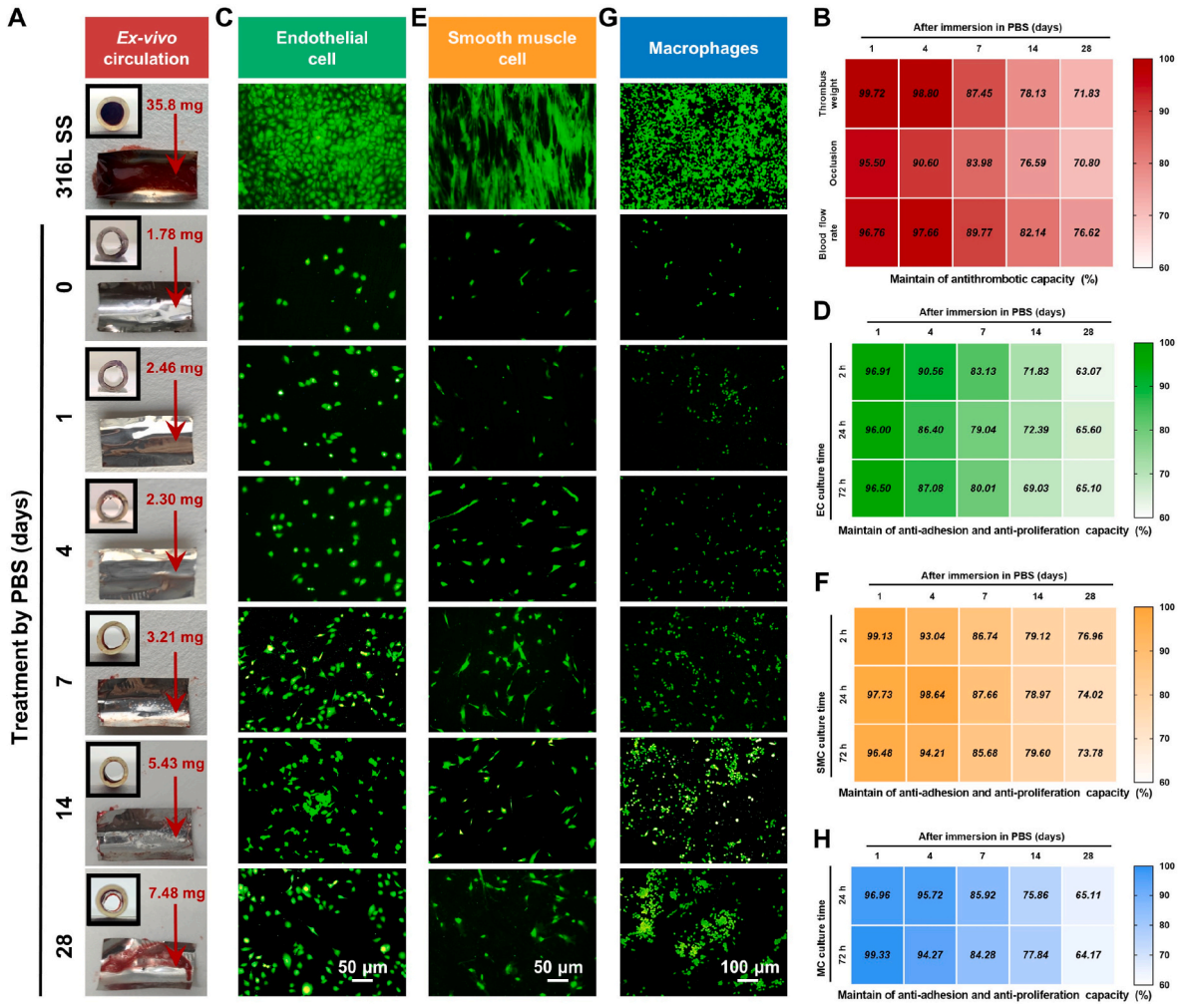

Fig. 7. Durability of the antifouling property of PEG-BSA@HCA. (A) Cross-sectional and surface images of pre-immersed 316L SS foils modified by PEG-BSA@HCA after circulation. (B) Heatmap of antithrombotic properties of PEG-BSA@HCA. Fluorescent images of (C) HUVECs, (E) HUASMCs, and (G) MCs adherent on PEG-BSA@HCA after 72 h of culture. Heatmap of anti-adhesion and anti-proliferation properties of PEG-BSA@HCA against (D) HUVECs, (F) HUASMCs, and (H) MCs.

CRediT authorship contribution statement

Nan Lyu: Writing – original draft, Visualization, Validation, Investigation, Funding acquisition, Formal analysis, Data curation. **Daihua Deng:** Writing – original draft, Methodology, Investigation. **Yuting Xiang:** Investigation. **Zeyu Du:** Visualization, Formal analysis. **Xiaohui Mou:** Investigation. **Qing Ma:** Investigation. **Nan Huang:** Supervision, Funding acquisition. **Jing Lu:** Supervision, Resources, Funding acquisition, Conceptualization. **Xin Li:** Methodology, Investigation, Formal analysis. **Zhilu Yang:** Writing – review & editing, Supervision, Resources, Funding acquisition, Conceptualization. **Wentai Zhang:** Writing – review & editing, Supervision, Resources, Funding acquisition.

Declaration of generative AI and AI-assisted technologies in the writing process

During the preparation of this work the author used ChatGPT 3.5 in order to polish the language of the article. After using this ChatGPT 3.5, the author(s) reviewed and edited the content as needed and take(s) full responsibility for the content of the publication.

Declaration of competing interest

Prof. Zhilu Yang is an editorial board member for Bioactive Materials and was not involved in the editorial review or the decision to publish this article. All authors declare that there are no competing interests.

Acknowledgments

We would like to sincerely thank Prof. Manfred F. Maitz (Leibniz Institute for Polymer Research, Dresden) for checking the article and his valuable comments. This work was supported by the National Natural Science Foundation of China, China (Project 82202325, 82072072, 32171326, 32261160372), the Guangdong Basic and Applied Basic Research Foundation, China (2022B1515130010, 2021A1515111035), Dongguan Science and Technology of Social Development Program, China (20231800906311, 20231800900332), China Postdoctoral Science Foundation, China (2022M721524). Leading Talent Project of Guangzhou Development District, China (2020-L013).

Appendix A. Supplementary data

Supplementary data to this article can be found online at https://doi.org/10.1016/j.bioactmat.2023.12.004.

References

[1] A. Stannard, J.L. Eliason, T.E. Rasmussen, Resuscitative endovascular balloon occlusion of the aorta (REBOA) as an adjunct for hemorrhagic shock, J. Trauma Acute Care Surg. 71 (6) (2011) 1869–1872.

[2] W. Wang, H. Li, M.D. Tam, D. Zhou, D.X. Wang, J. Spain, The amplatzer vascular plug: a review of the device and its clinical applications, Cardiovasc. Intervent. Radiol. 35 (4) (2012) 725–740.

[3] W. Xiu, S. Gan, Q. Wen, Q. Qiu, S. Dai, H. Dong, Q. Li, L. Yuwen, L. Weng, Z. Teng, Y. Mou, L. Wang, Biofilm microenvironment-responsive nanotheranostics for dual-mode imaging and hypoxia-relief-enhanced photodynamic therapy of bacterial infections, Research 2020 (2020), 9426453.

[4] B.S. Salter, C.R. Gross, M.M. Weiner, S.R. Dukkipati, G.W. Serrao, N. Moss, A. C. Anyanwu, D. Burkhoff, A. Lala, Temporary mechanical circulatory support devices: practical considerations for all stakeholders, Nat. Rev. Cardiol. 20 (4) (2023) 263–277.

[5] C.S. Joels, R.F. Sing, B.T. Heniford, Complications of inferior vena cava filters, Am. Surg. 69 (8) (2003) 654–659.

[6] N. Saito, H. Matsumoto, T. Yagi, Y. Hara, K. Hayashida, T. Motomura, K. Mashiko, H. Iida, H. Yokota, Y. Wagatsuma, Evaluation of the safety and feasibility of resuscitative endovascular balloon occlusion of the aorta, J. Trauma Acute Care Surg. 78 (5) (2015) 897–904.

[7] S.O. Trerotola, R.E. Pyeritz, Does use of coils in addition to amplatzer vascular plugs prevent recanalization? Am. J. Roentgenol. 195 (3) (2010) 766–771.

[8] H. Massoumi, M.K. Chug, G.H. Nguyen, E.J. Brisbois, A multidisciplinary experiment to characterize antifouling biocompatible interfaces via quantification of surface protein adsorption, J. Chem. Educ. 99 (7) (2022) 2667–2676.

[9] X. Mou, H. Zhang, H. Qiu, W. Zhang, Y. Wang, K. Xiong, N. Huang, H.A. Santos, Z. Yang, Mussel-inspired and bioclickable peptide engineered surface to combat thrombosis and infection, Research 2022 (2022), 9780879.

[10] Y. Hou, X. Deng, C. Xie, Biomaterial surface modification for underwater adhesion, Smart Materials in Medicine 1 (2020) 77–91.

[11] Q. Liu, P. Singha, H. Handa, J. Locklin, Covalent grafting of antifouling phosphorylcholine-based copolymers with antimicrobial nitric oxide releasing polymers to enhance infection-resistant properties of medical device coatings, Langmuir 33 (45) (2017) 13105–13113.

[12] B. Winkeljann, M.G. Bauer, M. Marczynski, T. Rauh, S.A. Sieber, O. Lieleg, Covalent mucin coatings form stable anti-biofouling layers on a broad range of medical polymer materials, Adv. Mater. Interfaces 7 (4) (2020), 1902069.

[13] B.M. Bakadia, L. Lamboni, A.A. Qaed Ahmed, R. Zheng, B.O. Ode Boni, Z. Shi, S. Song, T. Souho, B.M. Mukole, F. Qi, G. Yang, Antibacterial silk sericin/poly (vinyl alcohol) hydrogel with antifungal property for potential infected large burn wound healing: Systemic evaluation, Smart Materials in Medicine 4 (2023) 37–58.

[14] X. Hu, J. Tian, C. Li, H. Su, R. Qin, Y. Wang, X. Cao, P. Yang, Amyloid-like protein aggregates: a new class of bioinspired materials merging an interfacial anchor with antifouling, Adv. Mater. 32 (23) (2020), 2000128.

[15] J. Sabaté del Río, O.Y.F. Henry, P. Jolly, D.E. Ingber, An antifouling coating that enables affinity-based electrochemical biosensing in complex biological fluids, Nat. Nanotechnol. 14 (12) (2019) 1143–1149.

[16] D. Chan, J.-C. Chien, E. Axpe, L. Blankemeier, S.W. Baker, S. Swaminathan, V. A. Piunova, D.Y. Zubarev, C.L. Maikawa, A.K. Grosskopf, J.L. Mann, H.T. Soh, E. A. Appel, Combinatorial polyacrylamide hydrogels for preventing biofouling on implantable biosensors, Adv. Mater. 34 (24) (2022), 2109764.

[17] K. Li, J. Peng, Y. Liu, F. Zhang, D. Wu, R. Luo, Z. Du, L. Yang, G. Liu, Y. Wang, Surface engineering of central venous catheters via combination of antibacterial endothelium-mimicking function and fibrinolytic activity for combating blood stream infection and thrombosis, Adv. Healthc. Mater. 12 (23) (2023), 2300120.

[18] X. He, G. Sathishkumar, K. Gopinath, K. Zhang, Z. Lu, C. Li, E.-T. Kang, L. Xu, One-step self-assembly of biogenic Au NPs/PEG-based universal coatings for antifouling and photothermal killing of bacterial pathogens, Chem. Eng. J. 421 (2021), 130005.

[19] F. Song, L. Zhang, R. Chen, Q. Liu, J. Liu, J. Yu, P. Liu, J. Duan, J. Wang, Bioinspired durable antibacterial and antifouling coatings based on borneol fluorinated polymers: demonstrating direct evidence of antiadhesion, ACS Appl. Mater. Interfaces 13 (28) (2021) 33417–33426.

[20] Z. Wang, K. Wang, X. Lu, C. Li, L. Han, C. Xie, Y. Liu, S. Qu, G. Zhen, Nanostructured architectures by assembling polysaccharide-coated BSA nanoparticles for biomedical application, Adv. Healthc. Mater. 4 (6) (2015) 927–937.

[21] C. Hu, D.-P. Yang, F. Zhu, F. Jiang, S. Shen, J. Zhang, Enzyme-labeled Pt@BSA nanocomposite as a facile electrochemical biosensing interface for sensitive glucose determination, ACS Appl. Mater. Interfaces 6 (6) (2014) 4170–4178.

[22] D.P. Damera, S. Kaja, L.S.L. Janardhanam, S. Alim, V.V.K. Venuganti, A. Nag, Synthesis, Detailed characterization, and dual drug delivery application of BSA loaded aquasomes, ACS Appl. Bio Mater. 2 (10) (2019) 4471–4484.

[23] L. Wang, W. Gao, S. Ng, M. Pumera, Chiral protein-covalent organic framework 3D-printed structures as chiral biosensors, Anal. Chem. 93 (12) (2021) 5277–5283.

[24] S. Li, K. Wang, S. Hao, F. Dang, Z.Q. Zhang, J. Zhang, Antifouling gold-inlaid BSA coating for the highly efficient capture of circulating tumor cells, Anal. Chem. 94 (18) (2022) 6754–6759.

[25] C. Bhan, R. Mandlewala, A. Gebregeorgis, D. Raghavan, Adsorption-desorption study of BSA conjugated silver nanoparticles (Ag/BSA NPs) on collagen immobilized substrates, Langmuir 28 (49) (2012) 17043–17052.

[26] M. Fischer, C.P. Baptista, I.C. Gonçalves, B.D. Ratner, C. Sperling, C. Werner, C. L. Martins, M.A. Barbosa, The effect of octadecyl chain immobilization on the hemocompatibility of poly (2-hydroxyethyl methacrylate), Biomaterials 33 (31) (2012) 7677–7685.

[27] V. Hlady, J. Buijs, Protein adsorption on solid surfaces, Curr. Opin. Biotech. 7 (1) (1996) 72–77.

[28] Y. Han, Q. Shi, J. Hu, Q. Du, X. Chen, X. Jing, Grafting BSA onto poly[(L-lactide)-co-carbonate] microspheres by click chemistry, Macromol. Biosci. 8 (7) (2008) 638–644.

[29] S.D. Sinha, M. Choudhuri, T. Basu, D. Gupta, A. Datta, Decisive role of polymer-bovine serum albumin interactions in biofilm substrates on "philicity" and extracellular polymeric substances composition, Langmuir 38 (6) (2022) 1966–1976.

[30] J. Wei, W. Zhang, X. Mou, H. Meng, Q. Ma, W. Wang, X. Li, Q. Tu, W. Tian, N. Huang, Z. Yang, Bioinspired hemostatic and anti-Infective armor for wound healing assisted by metal-phenol-polyamine system, Adv. Funct. Mater. 2306267..

[31] S.C. Goh, Y. Luan, X. Wang, H. Du, C. Chau, H.E. Schellhorn, J.L. Brash, H. Chen, Q. Fang, Polydopamine-polyethylene glycol-albumin antifouling coatings on multiple substrates, J. Mater. Chem. B 6 (6) (2018) 940–949.

[32] P. Gao, H. Qiu, K. Xiong, X. Li, Q. Tu, H. Wang, N. Lyu, X. Chen, N. Huang, Z. Yang, Metal-catechol-(amine) networks for surface synergistic catalytic modification: therapeutic gas generation and biomolecule grafting, Biomaterials 248 (2020), 119981.

[33] S. An, E.J. Jeon, S.Y. Han, J. Jeon, M.J. Lee, S. Kim, M. Shin, S.-W. Cho, pH-Universal catechol-amine chemistry for versatile hyaluronic acid bioadhesives, Small 18 (41) (2022), 2202729.

[34] Y. Wang, E.J. Jeon, J. Lee, H. Hwang, S.-W. Cho, H. Lee, A phenol-amine superglue inspired by insect sclerotization process, Adv. Mater. 32 (43) (2020), 2002118.

[35] Y. Yu, X. Li, J. Li, D. Li, Q. Wang, W. Teng, Dopamine-assisted co-deposition of hydroxyapatite-functionalised nanoparticles of polydopamine on implant surfaces to promote osteogenesis in environments with high ROS levels, Mater. Sci. Eng. C 131 (2021), 112473.

[36] T. Drobek, N.D. Spencer, Nanotribology of surface-grafted PEG layers in an aqueous environment, Langmuir 24 (4) (2008) 1484–1488.

[37] C. Allen, N. Dos Santos, R. Gallagher, G.N.C. Chiu, Y. Shu, W.M. Li, S.A. Johnstone, A.S. Janoff, L.D. Mayer, M.S. Webb, M.B. Bally, Controlling the physical behavior and biological performance of liposome formulations through use of surface grafted poly(ethylene Glycol), Biosci. Rep. 22 (2) (2002) 225–250.

[38] X. Ding, C. Yang, T.P. Lim, L.Y. Hsu, A.C. Engler, J.L. Hedrick, Y.-Y. Yang, Antibacterial and antifouling catheter coatings using surface grafted PEG-b-cationic polycarbonate diblock copolymers, Biomaterials 33 (28) (2012) 6593–6603.

[39] J. Wang, C.J. Pan, N. Huang, H. Sun, P. Yang, Y.X. Leng, J.Y. Chen, G.J. Wan, P. K. Chu, Surface characterization and blood compatibility of poly(ethylene terephthalate) modified by plasma surface grafting, Surf. Coat. Technol. 196 (1) (2005) 307–311.

[40] K.C. Popat, S. Sharma, T.A. Desai, Quantitative XPS analysis of PEG-modified silicon surfaces, J. Phys. Chem. B 108 (17) (2004) 5185–5188.

[41] S. Sharma, R.W. Johnson, T.A. Desai, XPS and AFM analysis of antifouling PEG interfaces for microfabricated silicon biosensors, Biosens. Bioelectron. 20 (2) (2004) 227–239.

[42] I. Evangelista, D. Wencel, S. Beguin, N. Zhang, M.D. Gilchrist, Influence of surface texturing on the dry tribological properties of polymers in medical devices, Polymers 15 (13) (2023) 2858.

[43] S. Nagaoka, R. Akashi, Low-friction hydrophilic surface for medical devices, Biomaterials 11 (6) (1990) 419–424.

[44] X. Zhang, Y. Zhang, Z. Jin, A review of the bio-tribology of medical devices, Friction 10 (1) (2022) 4–30.

[45] M.K. Singh, Polymer brush based tribology, in: J.K. Katiyar, P. Ramkumar, T. Rao, J. Davim (Eds.), Tribology in Materials and Applications, Springer, Cham, 2020, pp. 15–32.

[46] R.J. Narayan, P.N. Kumta, C. Sfeir, D.-H. Lee, D. Choi, D. Olton, Nanostructured ceramics in medical devices: applications and prospects, JOM 56 (10) (2004) 38–43.

[47] B.T. Houseman, M. Mrksich, The microenvironment of immobilized Arg-Gly-Asp peptides is an important determinant of cell adhesion, Biomaterials 22 (9) (2001) 943–955.

[48] G. Zhou, T. Groth, Host responses to biomaterials and anti-Inflammatory design-a brief review, Macromol. Biosci. 18 (8) (2018), 1800112.

[49] J.M. Anderson, S. Jiang, Implications of the acute and chronic inflammatory response and the foreign body reaction to the immune response of implanted biomaterials, in: B. Corradetti (Ed.), The Immune Response to Implanted Materials and Devices, Springer, Cham, 2017, pp. 15–36.

[50] H. Li, Q. Guo, Q. Tu, K. Xiong, W. Wang, L. Lu, W. Zhang, N. Huang, Z. Yang, Nitric oxide-generating self-assembling peptide hydrogel coating for enhancing hemocompatibility of blood-contacting devices, J. Mater. Sci. Technol. 131 (2022) 106–114.

[51] Y. Liu, F. Zhang, S. Lang, L. Yang, S. Gao, D. Wu, G. Liu, Y. Wang, A uniform and robust bioinspired zwitterion coating for use in blood-contacting catheters with improved anti-inflammatory and antithrombotic properties, Macromol. Biosci. 21 (12) (2021), 2100341.

[52] Z. Yang, X. Zhao, R. Hao, Q. Tu, X. Tian, Y. Xiao, K. Xiong, M. Wang, Y. Feng, N. Huang, G. Pan, Bioclickable and mussel adhesive peptide mimics for engineering vascular stent surfaces, Proc. Natl. Acad. Sci. 117 (28) (2020) 16127–16137.